The Muon Portal Double Tracker for the Inspection of Travelling Containers

C. Pugliatti, V. Antonuccio, M. Bandieramonte, U. Becciani, F. Belluomo, A. Blancato, G. Bonanno, A. Costa, P. G. Fallica, S. Garozzo, A. Grillo, V. Indelicato, P. La Rocca, E. Leonora, F. Longhitano, S. Longo, D. Lo Presti, D. Marano, P. Massimino, C. Petta, C. Pistagna, M. Puglisi, N. Randazzo, F. Riggi, S. Riggi, G. Romeo, G. V. Russo, G. Santagati, M.C. Timpanaro, G. Valvo, F. Vitello, and A. Zaia

***Abstract*—The Muon Portal Project has as its goal the design and construction of a real-size working detector prototype in scale 1:1, to inspect the content of travelling containers by means of the secondary cosmic-ray muon radiation and to recognize high-Z hidden materials (i.e. U, Pu). The tomographic image is obtained by reconstructing the input and output trajectories of each muon when it crosses the container and, consequently, the scattering angle, making use of two trackers placed above and below the container. The scan is performed without adding any external radiation, in a reasonable time (few minutes) and with a good spatial and angular resolution. The detector consists of 8 planes each segmented in 6 identical modules. Each module is made of scintillating strips with two WaveLength Shifting fibers (WLS) inside, coupled to Silicon photomultipliers. The customized read-out electronics employs programmable boards. Thanks to a smart read-out system, the number of output channels is reduced by a factor 10. The signals from the front-end modules are sent to the read-out boards, in order to convert analog signals to digital ones, by comparison with a threshold. The data are pre-analyzed and stored into a data acquisition PC. After an intense measurement and simulation campaign to carefully characterize the detector components, the first detection modules (1×3 m^2) have been already built. In this paper the detector architecture, particularly focusing on the used electronics and the main preliminary results will be presented.**

***Index Terms*—Muon detectors, particle tracking, safety systems.**

I. Introduction

THE yearly traffic of containers, employed in ports all around the world for the safe storage and transport of materials by ships, is constantly growing up. It is estimated in 200 Millions containers per year, but inspection procedures are applied to only 1% of them, because of prohibitive inspection times and high costs. The most common scanning technique is the X-ray radiography. It requires an external source, which introduces additional radiation levels in the environment and it is ineffective when crossing very dense objects, due to the radiation absorption phenomena.

The application of alternative techniques, such as directional gamma imaging and neutron radiography, is complex and expensive, and the performances can be seriously degraded in presence of shielding materials.

The growing demand for more stringent safety regulations requires scanning of all transiting containers, however.

Worldwide, several Projects have been proposed with the aim of building similar detector prototypes [1]–[8].

The Muon Portal Project [9] is a new Project in this field, based on cosmic muon tomography.

The Project is aimed at building a complete tomographer prototype, specifically designed for the identification and localization of high-Z materials hidden inside containers.

With respect to traditional inspection techniques, muon tomography has some advantages. For example, the scan operation is not invasive (it is not necessary to open the container), and the use of cosmic rays does not imply the use of additional radiation sources, dangerous for the environment. The acquisition time may be reduced to few minutes, and the content is not damaged because muons are a natural source of radiation.

The detection technique is based on the determination of the scattering angle of cosmic muons induced by heavy materials, when crossing the particle trackers. Indeed, the scattering angle is particularly sensitive to the atomic number Z of the crossed material. Consequently a system for muon tomography requires two tracking detectors, above and below the volume to be inspected.

Manuscript received June 10, 2014; revised December 24, 2014; accepted October 30, 2015. Date of current version December 11, 2015. This work was supported by the Muon Portal Collaboration: http://muoni.oact.inaf.it:8080.

C. Pugliatti and V. Indelicato are with the Department of Physics and Astronomy, University of Catania, via Santa Sofia 64, 95123 Catania, Italy and also with the INFN, Sezione di Catania, 95123 Catania, Italy.

V. Antonuccio, M. Bandieramonte, U. Becciani, G. Bonanno, A. Costa, A. Grillo, D. Marano, P. Massimino, C. Pistagna, G. Romeo, M.C. Timpanaro, and F. Vitello are with the INAF, Osservatorio Astrofisico Catania, Catania, Italy.

F. Belluomo and M. Puglisi are with the Meridionale Impianti, Catania, Italy.

S. Garozzo is with the Osservatorio Astrofisico di Catania, INAF - Istituto Nazionale di AstroFisica, Catania, Italy.

A. Blancato, P. La Rocca, C. Petta and G. Santagati are with the Dept. of Physics and Astronomy, University of Catania, Catania, Italy.

P. G. Fallica and G. Valvo are with the STMicroelectronics, Catania, Italy.

E. Leonora is with the Dep. of Physics and Astronomy, INFN, section of Catania, 95123 Catania, Italy.

F. Longhitano is with the Sezione di Catania, Istituto Nazionale di Fisica Nucleare, Catania, Italy.

S. Longo and A. Zaia are with the Insirio, Catania, Italy.

D. Lo Presti is with the Dipartimento di Fisica ed Astronomia, University degli studi di, Catania, I95123, Italy.

N. Randazzo is with the INFN, Catania, 95123 Catania, Italy.

F. Riggi is with the Dept. of Physics and Astronomy, University of Catania, 95123 Catania, Italy.

S. Riggi is with the Osservatorio Astrofisico Catania, INAF, 95123 Catania, Italy.

G. V. Russo is with the University di Catania, Fisica ed Astronomia, 95125 Catania, Italy.

Color versions of one or more of the figures in this paper are available online at http://ieeexplore.ieee.org.

Digital Object Identifier 10.1109/TNS.2015.2497079

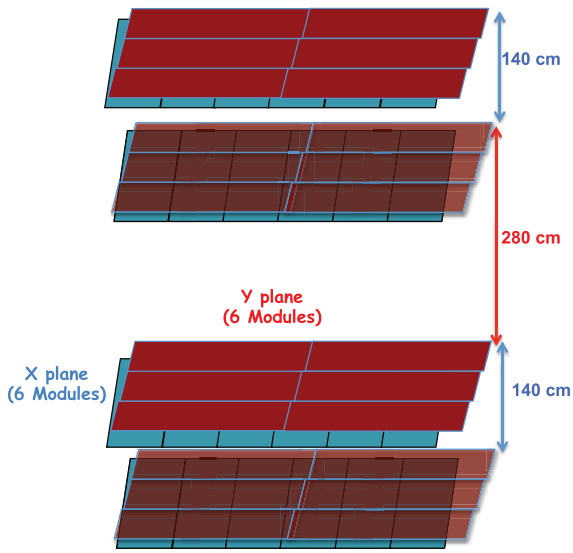

Fig. 1. Sketch of the detector layout. Two trackers consisting of eight detection planes, with 6 modules for each are visible.

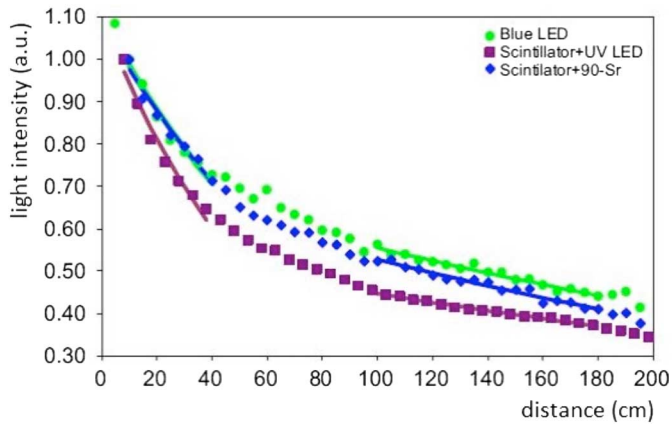

Fig. 2. Kuraray Y11 (200) response to different sources, with and without an external scintillator.

II. Detector Architecture

The detector design, sketched in Fig. 1, includes four X-Y planes of dimension 3×6 m^2 corresponding to eight physical planes. It is suitable for a full inspection of a real TEU (Twenty-foot Equivalent Units) container ($244 \times 259 \times 610$ cm^3).

Six identical modules (1×3 m^2 size) are suitably placed on each plane in order to cover both the X and Y coordinates with a modular structure, minimizing the dead area, which is in the order of 0.1% of the total sensitive area. Each module consists of 100 extruded plastic scintillator strips ($1 \times 1 \times 300$ cm^3). Two Wave-Length Shifting (WLS) fibers, placed on each strip to transport the light produced by the crossing particles are optically and mechanically coupled to the photo-sensor placed at one of the fiber ends. The detection planes of each tracker are 140 cm spaced, while the inner planes are separated by about 280 cm, so that it is possible to insert a standard container. In this way, the spatial resolution, which is of the order of $10/\sqrt{12}$ mm ≈ 3.5 mm, is suitable to provide a good tracking capability for each muon, allowing the reconstruction of the incoming and outgoing tracks and, consequently, the scattering angle with a geometrical angular resolution of about 0.2 degrees [10].

The detection planes are supported by a suitable mechanical structure, with the aim of minimizing the amount of traversed material by the charged particles. The mechanical structure is made by 6 pillars in iron steel (few cm thickness) with a light metal grid for each detection plane. The effect of the structure on the muon scattering has been included in the GEANT4 simulation and the additional amount of muon scattering due to the structure on the image reconstruction found to be negligible.

III. Optimization of Light Collection

The use of WLS fibers to transport the light produced in the scintillating strips greatly reduces the light absorption along the strip and allows to adapt the wavelength of the emitted light to more appropriate values close to the region of the photo-sensors maximal sensitivity. In order to choose the best configuration for the final detector design and to optimize the light collection at one end of the strip a series of experimental tests have been carried out on several prototypes of scintillator strips and WLS fibers from different suppliers. Among the strip prototypes with 1 cm^2 cross-section, we tested various configurations, i.e. with a centered hole able to accommodate two 1 mm WLSs, as well as strips with two 1 mm grooves put on the same side. The latter is the final chosen configuration. Following the tests results we decided to use for the Project the Kuraray Y11 (200) fibers, which have shown the best performances in terms of number of photoelectrons detected by a suitable photo-sensor, varying the distance of the particle impact point from it (details in Ref. [11][12]).

Test measurements and GEANT4 simulations were carried out on different strip and fiber prototypes, also to study the transport of optical photons to the photosensors [13]. The intensity of the light reaching the photosensor along the WLS fibers $I(x)$ is often parameterized as a function of the distance x as:

$$I(x) = I_0 \left(a e^{-\frac{x}{\lambda_s}} + b e^{-\frac{x}{\lambda_l}} \right). \quad (1)$$

where λ_s and λ_l are the short and long attenuation lengths respectively, and I_0 is the intensity at the emission point.

For WLS fibers, λ_s is usually a few tens of cm, and its effect is strongly reduced at large distances. Fig. 2 shows the Kuraray Y11 (200) response to three different sources, as a function of the distance: a blue LED light directly injected into the fiber, an UV LED and electrons from a ^{90}Sr source hitting a scintillator. As it can be seen, the light intensity follows a nearly exponential trend for all the sources, with some evidence of the short component at small distances ($x < 50$ cm). Concerning the number of photons obtained at the photo-sensor, these have been evaluated through GEANT4 simulations [13] and the results allow to conclude that a reasonable value of the threshold (of the order of 2-3 photoelectrons) is a reasonable choice in order to have a high efficiency and a moderate Dark Count Rate DCR of the Silicon Photomultipliers.

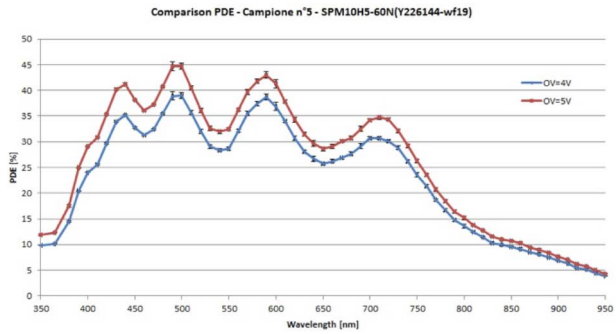

Fig. 3. PDE measurement comparison at OV $=$ 4 V and OV $=$ 5 V and temperature T $=$ 28°C.

TABLE I
SiPM Properties

Parameter	Unit	Value
Array size	μm²	3968 × 4464
Array dimension		64 × 72
Number of cells in one pixel		1145
Cell fill factor	%	47.0
Cell size	μm²	62.0 × 62.0
Diode pad area	μm²	122 × 100
Pixel pad area	μm²	124 × 124

Main characteristics of the Silicon photomultipliers employed in the present investigation (STMicroelectronics Mod. 4SPM20-62N).

IV. The Photo-sensor

It was decided to use custom designed SiPMs to convert the scintillating light into an electrical signal. Different SiPM prototypes, both with the p on n and n on p technologies were produced and tested by ST Microelectronics in order to maximize the photon Detection Efficiency (PDE), the fill factor with a low cross-talk and DCR.

Fig. 3 shows the comparison between PDE measurements carried out at two values of Over Voltage (OV) on a SiPM device similar to the one that will be used for the Project.

The final chip indeed is a n on p one, with 4 SiPMs: two couples respectively with pixel size 60 um and 75 um. The PDE is about 40% and the fill factor 67%.

The main characteristics of the package are reported in Table I.

The layout of the final chip that will be employed for the Project is shown in Fig. 4.

The photo-sensor that has to be employed in the Muon Portal Detector requires an appropriated design to be adapted to the mechanical requirements and the optical properties of the strips and the WLS fibers. Therefore the SiPMs have been designed with a higher fill-factor, smaller cells and a larger gain. The size of the SiPM will be circular with a diameter of about 1.5 mm (Fig. 4). The distance between the centers of the two SiPMs is chosen to optimize the coupling with the two fibers.

A batch of $\sim$ 10000 SiPMs has been produced and encapsulated in a Surface Mount Optical (SMD) package. A custom procedure has been implemented for the characterization of such devices. The device to be tested with its proper socket is placed inside a black box and then biased by a Keithley picoammeter/

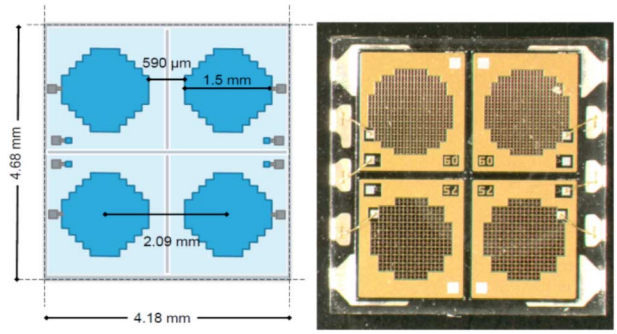

Fig. 4. Layout (left) and picture (right) of the SiPM chip MUON-60 (60 μm $\times$ 60 μm is the single cell size, while the diameter of the total circular sensitive is 1.5 mm), foreseen for the Muon Portal Detector, designed by STMicroelectronics. Only 2 of the 4 SiPMs will be used for each strip.

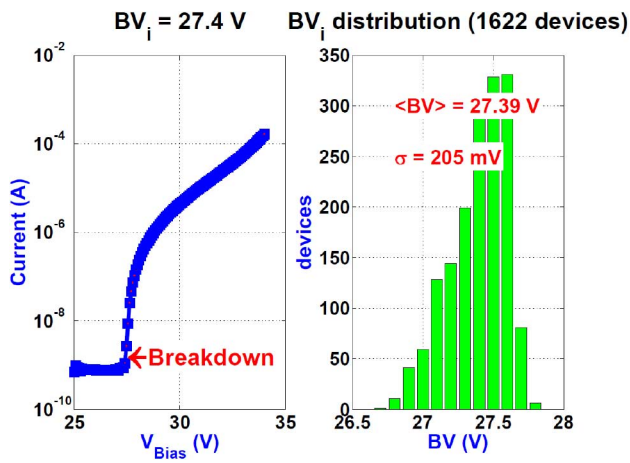

Fig. 5. (Left) I-V characteristics curve for one of the MUON60 devices. (Right) BV distribution for a sample of 1622 devices already tested.

voltage source [14]. The Keithley was also used to read the current from the SiPM and transmit the data to a PC. In order to measure the complete I-V curve in an automatic way by setting the bias voltage and reading the corresponding current in the device, a LabVIEW program has been developed, in order to find the Breakdown Voltage (BV) value for each SiPM under test. After the construction of the I-V curve those SiPMs which do not satisfy stringent criteria on the BV are rejected. Other testing criteria are applied to the BV $+$ 5 V and the BV $-$ 2 V corresponding current values. The goodness of a device is evaluated in a simple way, thanks to the switching of appropriate signaling LEDs [15].

In Fig. 5, on the left, the I-V characteristics curve for one of the SiPMs under test is shown. The BV is 27.4 V. On the right the BV distribution for a sample of 1622 devices already tested is shown. The Gaussian mean value is 27.4 V with a standard deviation of 0.2 V.

An additional characterization of the final chips was performed on a limited sample of devices, illuminating them with a blue light driven from a pulsed LED through an optical fibre, inside a light-tight box. The output signal from each biased SiPM was amplified by the use of a CAEN SP5600 General Purpose Power Supply and Amplification Unit. A CAEN DT5720A fast digitizer (2 Channels, 250 MS/ s, 12 bit) allowed to display the signals, evaluate the output charge of the sensor

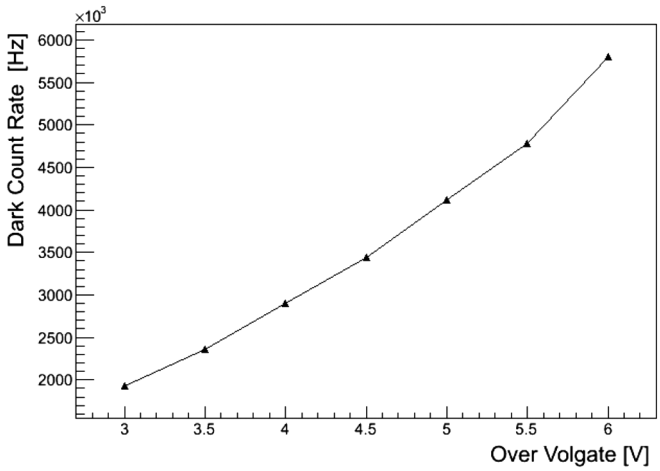

Fig. 6. Dark count rate of MUON60 SiPM as a function of overvoltage. Data were obtained at a room temperature of 23°C.

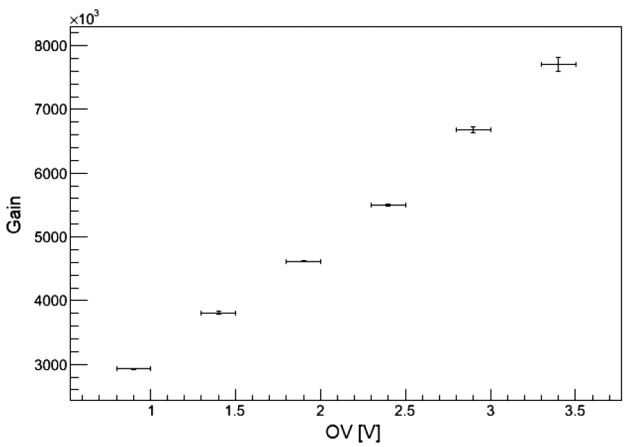

Fig. 7. Gain of MUON60 as a function of overvoltage. It includes the direct and indirect crosstalk contributions.

under test and measure the DCR in absence of light. All these data were processed to extract additional information, such as the gain and the resolution power of the system. As an example, the DCR as a function of the overvoltage is reported in Fig. 6, whereas Fig. 7 shows the gain of MUON-60 as a function of the OV [16].

V. Read-out of the Signals

The SiPMs are read using a suitable front-end electronics (Fig. 8). A front-end box for each module of the detector planes is provided. It accommodates the SiPMs, the power supply and temperature control system, the front-end electronics, a connector for the front-end functional parameters control and for the interface to the acquisition electronics.

The use of SiPM sensors to measure the signals coming from the fibers, requires a remote adjustable power supply, able to compensate the variations of the intrinsic characteristics (gain, PDE, dark current) caused by the environment.

The power supply section and the temperature controller are able to stabilize the working points of the SiPMs, which were suitably selected to have almost identical characteristics.

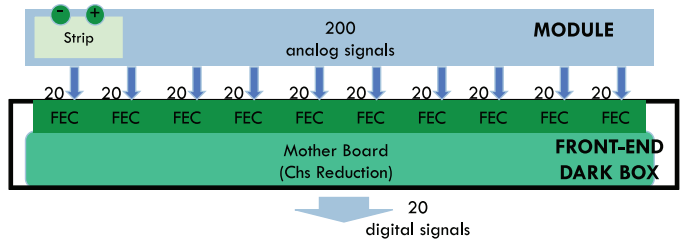

Fig. 8. Front-end block diagram.

The temperature conditioning (sensors and actuators), power supply and the control and communication (Gbs Ethernet) systems are managed by a unique Semi-Custom Front-end chip (FPGA and Front-end). The front-end modules also include lines drivers and amplifiers in addition to the mechanical housings.

For each detector module, the channels are read by 200 SIPMs housed into ten Front-End Cards (FECs). The 20 signals arriving to a FEC, sorted two by two in correspondence of each strip, are amplified about 30 times by a very fast operational amplifier, the THS3201 (1.8 GHz GBW). The resulting single photoelectron signal is about 27 mV in amplitude and 20 ns wide (at OV of about 2.4 V). All FECs are connected to a main board, unique for each module. There, a reduction channel strategy is applied [17]. Indeed, 10 neighboring analog signals of a FEC, one signal for each strip, are summed and amplified 3 times by another THS3201. The analogue outputs of the other remaining SiPMs of the FEC are then summed to signals of the same order (1st, 2nd, etc…) coming from the other FECs and amplified by a factor 3.

Thanks to the smart read-out strategy the output channels are reduced by a factor 10, for a total of $2\sqrt{100} = 20$ output signals for each module.

The 20 signals from each module are then compared to user-defined thresholds. Then, they are stretched by monostables (100 ns). After passing the monostables, the 120 signals from a plane are sent to a NI PXI-7813R board with 160 Digital I/O. The 40 remaining board lines are used to adjust the thresholds of the DAQ.

The programmable logic VIRTEX-II FPGA Module 40 MHz, housed into the board, samples the outputs from the front end module, decodes the hit strip and produces a label frame for each event. The data are pre-analyzed and stored into a data acquisition PC. For the read-out of the overall detector, 8 National Instruments PXI-7813R boards, a real-time module (NI PXIe-8135) used to correlate the signals from all the detection planes, and a GPS module (NI PXI-6682) for the synchronization are needed, housed into a suitable crate, which houses the controller together with the FPGA boards. The acquisition software triggers only coincident events in all the four detector planes (coincidence gate of 50 ns).

VI. Simulations

A. Detector Simulation and Cosmic Rays Generation

Detailed GEANT4 simulations have been performed in order to understand and reproduce the performance of our detector

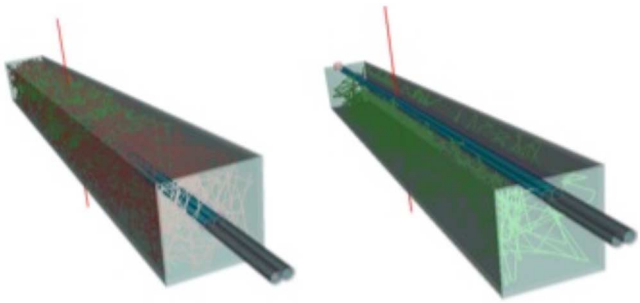

Fig. 9. Sketch of possible designs of extruded scintillator strips with two WLS housed into two groves.

and to optimize the algorithms for the reconstruction of the tomographic image [18][19].

The main ingredients of the simulations include the implementation of a full replica of the detector, with its mechanical support and with a container inside; the generation of a realistic cosmic rays distribution (using the CORSIKA code); the transport of optical photons fully simulated and then parameterized to save CPU time; the reconstruction of hits and clusters, including those due to electromagnetic showers. In Fig. 9 a sketch of possible designs of extruded scintillator strips with two WLS housed into two groves is shown. The configuration with two 1 mm grooves located on the same side is the final configuration chosen.

B. Reconstruction Algorithms

The output of the GEANT4 simulations has been used to implement several algorithms for the reconstruction of the tomographic image.

The simplest method to reconstruct the tomographic image is the POCA (Point Of Closest Approach) algorithm. It finds the point of closest approach between the incoming and the outgoing tracks of each crossing muon. Consequently it is possible to estimate the scattering point as the centroid between the points of closest approach. However, this algorithm ignores any underlying physics of scattering such as multiple scattering events, assuming that the scattering happens in a single point.

A modified version of the Friends-Of-Friends (FOF) clustering algorithm, unsupervised and multi-steps, has been also implemented [13]. It is a density-based algorithm, which elaborates the data independently from the grid and the 3D voxels and shows good performance acting as a noise filter especially useful in very dense scenarios.

Finally the EM-ML (Expectation Maximization-Maximum Likelihood) method is an iterative algorithm based on the subdivision of the entire volume to be inspected in k voxels (characterized by a density of scattering λ_{k}). Thanks to iterative procedures to maximize log-likelihood, it is possible to find the best set of the parameters λ_{k}. Even if the computation time is still prohibitive for a real application, a parallel implementation (applied both in the initialization and imaging step of the algorithm) will be soon ready to allow a real time application of the method even with a modest number of computing machines.

The algorithms have been tested and optimized over different simulation scenarios. As an example we supposed to scan a 20' empty container with "MUON" shape placed at the center, built with voxels of size 10 cm $\times$ 10 cm $\times$ 10 cm (Fig. 10). Each letter is made of a different material: $\mathrm{M} = \mathrm{Uranium}$, $\mathrm{U} = \mathrm{Iron}$, $\mathrm{O} = \mathrm{Lead}$, $\mathrm{N} = \mathrm{Aluminum}$. The shape is surrounded (thus hidden) by layers of washing machine-like elements, made of an aluminum casing and an iron engine inside, with relative support bars and a concrete block. Each tomographic reconstructed image supposes a statistics of 1 million reconstructed events (corresponding to about 10 minutes of data taking). A realistic energy distribution of the incoming muons has been assumed, as derived by CORSIKA simulation. Of course, the amount of scattering suffered by muons depends on their energy, so that the obtained results are the convolution of the 3D tomographic images with the realistic energy distribution. With all the methods, it is clearly possible to distinguish the M and O letters, made by elements with higher atomic numbers (Uranium and Lead). The POCA and the FOF reconstruction algorithms show a persistent halo that slightly increases the size of the letters, especially along the vertical direction. It is a consequence of the basic assumptions of the POCA algorithm, used as input for the FOF. In every case, the EM-ML algorithm reconstructs the target objects with a considerably better resolution. However, the noise induced by the presence of the washing machines is present in the POCA and EM-LM volume renderings while is considerably reduced by the use of the FOF density-based algorithm.

VII. Preliminary Tests of a Detection Module

This section presents the first tests results concerning one of the complete modules of the Muon Portal detector. The module was placed on a suitable supporting table, at room temperature (23°C). In order to reduce the noise due to the SiPM dark count rate, the coincidence between the two SiPMs connected to the same strip was imposed during the acquisition.

At first, several calibration measurements of the single photoelectron amplitude were performed varying the bias voltage V_{bias}. The results are reported in Table II.

Fixing the SiPMs power supply at $V_{bias} = 30$ V, which corresponds to an OV of 2.6 V (considering $\mathrm{BV} = 27.4$ V as reported in Section IV) the dark current rate at room temperature was measured. It is of the order of 100 kHz for a threshold of 1 p.e.. At 2 p.e. it is reduced to a few kHz.

A plastic scintillator (sensitive area $12 \times 12 \times 1$ cm^3) was placed 4.5 cm above an AMCRYS strip surface. The coincidence rate of cosmic rays events between the sensor and the scintillator signals was acquired varying the distance from the SiPM, for a fixed threshold (2.5 p.e.), and $\mathrm{V_{bias}} = 30$ V. The results are reported in Fig. 11.

As follows from Fig. 11 the coincidence rate is fairly constant along the overall length of the strip.

A procedure of channels equalization was performed by properly setting the SiPM thresholds, in order to minimize differences for the spurious coincidence rates for all channels of a complete module under test. Using the same external trigger scintillator, the coincidences between this detector and the overall module (100 strips) were measured. A typical result is shown in Fig. 12, where the peak due to the position of the scintillator along the short side (1 m) of the module is seen. In case of two close strips hit in the event, an average of the

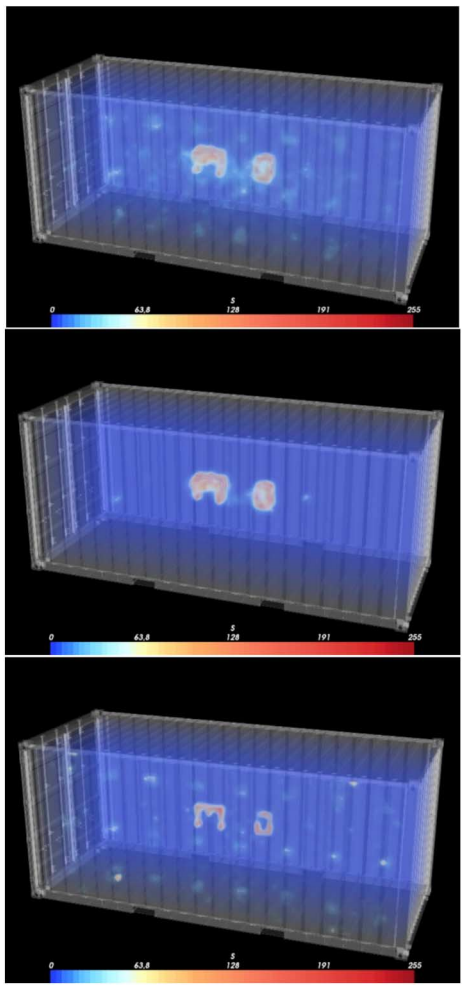

Fig. 10. Results of the reconstruction algorithms applied to a simulated scenario. From top to bottom: the POCA, the modified unsupervised Friends-of-Friends and the EM-LM.

TABLE II
SINGLE PHOTOELECTRON AMPLITUDES

Bias Voltage (Volt)	Amplitude (mV)
29.5	20
30	30
31	50

Single photoelectron amplitudes at different biasing voltages.

two strip positions was assumed, with proper smearing due to the strip size. As it is seen, spurious coincidences are very low on the two sides of the peak. Moreover, it is important to underline that, even if each individual SiPM is quite noisy at low thresholds, the 8-fold coincidence between the detection planes allows minimizing the spurious coincidence rate.

As a result of the measurements reported in Fig. 11 and Fig. 12, a rough estimate of the average hit efficiency was found to be close to 100%, taking into account the geometry of the trigger scintillator with respect to the detector module, and considering a small value of the threshold (around 2 p.e.), which is reasonable due to an average number of photoelectrons around 6-7, even at the largest distance from the photosensor.

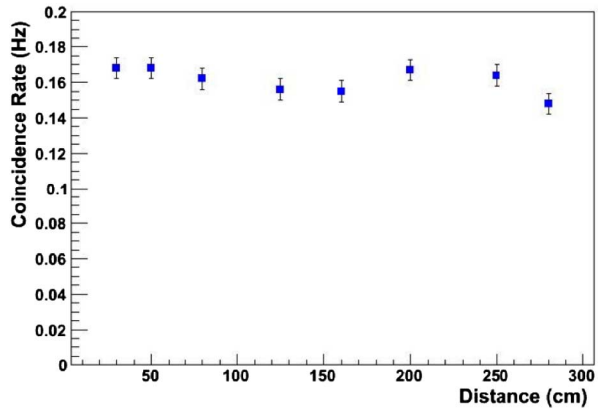

Fig. 11. Coincidence rate of a plastic scintillator and the strip under test as a function of distance from the SiPM with threshold 2.5 p.e. (1 p.e. $=$ 30 mV) and $V_{bias} = 30$ V. The employed strips are the Amcrys (3 m long) with Kuraray Y11 (200) fibers embedded.

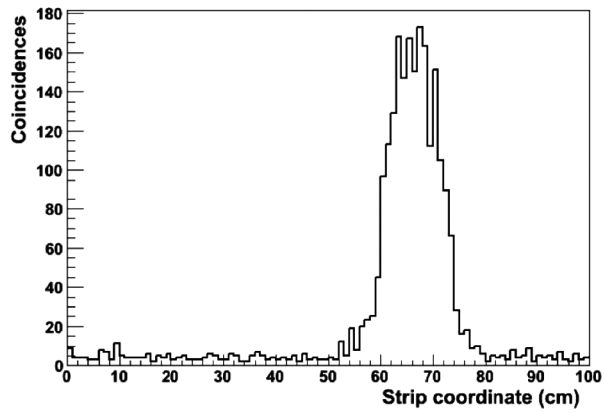

Fig. 12. Cosmic rays coincidence events for a complete module under test as a function of the distance expressed in strip number.

A more detailed investigation of the point-to-point hit and tracking efficiency will be done with the detection modules fully installed, profiting of the possibility to track the muons by three X-Y planes and looking at the associated hits on the fourth plane.

VIII. CONCLUSIONS

The Muon Portal Collaboration has designed and is building a portal prototype based on muon tomography for the identification and localization of materials with high atomic number hidden inside containers.

The design of the detector architecture, a simulation campaign on the detector response, the preliminary tests on individual components (strips, WLS fibers, SiPM) were carried out in order to obtain the best performances for an optimal reconstruction. As a result of such tests, the final detector components were chosen.

Image reconstruction algorithms employing different methods are almost ready. After a R&D phase, the construction of the complete detector has already started. More than 50% of the detection modules are now built, together with the front-end electronics and read-out systems. The mechanical structure is now ready to accommodate the detection planes, and the setup will be ready within mid 2016.

ACKNOWLEDGMENT

This work is supported by the Muon Portal Collaboration. The partners of the Project are:

- Department of Physics & Astronomy, University of Catania
- INAF–Astrophysical Observatory of Catania
- STMicroelectronics, Catania
- Meridionale Impianti Welding Technology, Catania
- Insirio SPA, Messina

REFERENCES

[1] K. Gnanvo *et al.*, "Imaging of high-Z material for nuclear contraband detection with a minimal prototype of a muon tomography station based on GEM detectors," *Nuclear Instruments & Methods in Physics Research Section A*, vol. 652, pp. 16–20, Oct. 2011.

[2] W. Priedhorsky *et al.*, "Detection of high-Z objects using multiple scattering of cosmic ray muons," *Review of Scientific Instruments*, vol. 74, Sep. 2003.

[3] A. Clarkson *et al.*, "The design and performance of a scintillating-fibre tracker for the cosmic-ray muon tomography of legacy nuclear waste containers," *Nuclear Instruments & Methods in Physics Research Section A*, vol. 745, pp. 138–149, May 2014.

[4] S. Pesente *et al.*, "First results on material identification and imaging with a large-volume muon tomography prototype," *Nuclear Instruments & Methods in Physics Research Section A, Accelerators, Spectrometers, Detectors and Associated Equipment*, vol. 604, p. 738, Jun. 2009.

[5] Y. Qian *et al.*, "Study on the performance of large area MRPC with high position resolution," *Nuclear Instruments & Methods in Physics Research Section A*, vol. 661, pp. S159–S162, Jan. 2012.

[6] D. Waller *et al.*, A simulation study of the cosmic ray inspection and passive tomography (CRIPT) muon spectrometer Technical Memorandum DRDC Ottawa TM 2010-168, Oct. 2010.

[7] L. J. Schultz *et al.*, "Image reconstruction and material Z discrimination via cosmic ray muon radiography," *Nuclear Instruments & Methods in Physics Research Section A*, vol. 519, no. 3, pp. 687–694, Mar. 2014.

[8] L. Cox *et al.*, "Detector requirements for a cosmic ray muon scattering tomography system," in *IEEE Nuclear Science Symposium and Medical Imaging Conference (2008 NSS/MIC)*, 345 E 47TH ST, New York, USA, 2008, vol. 1–9.

[9] The Muon Portal Collaboration. Muon Portal Project [Online]. Available: http://muoni.oact.inaf.it::8080/

[10] F. Riggi *et al.*, The Muon Portal Collaboration, "The muon portal project: Development of an innovative scanning portal based on muon tomography," in *Proc. the ANIMMA 2013 Conference*, Marseille, Jun. 2013, pp. 23–27.

[11] M. Dracos *et al.*, The OPERA Collaboration, "The OPERA experiment," *Physics of Atomic Nuclei*, vol. 67, no. 6, pp. 1092–1096, Jun. 2004.

[12] G. V. Russo *et al.*, "Strip detectors for a portal monitor application," *J. Instrumentation (JINST)*, vol. 9, p. P11008, Nov. 2014.

[13] S. Riggi *et al.*, The Muon Portal Collaboration, "Geant4 simulation of plastic scintillator strips with embedded optical fibers for a prototype of tomographic system," *Nuclear Instruments & Methods in Physics Research Section A*, vol. 624, pp. 583–590, Dec. 2010.

[14] The Keithley current and voltage sourcing [Online]. Available: http://www.keithley.com/products/currentvoltage/voltagecurrentsourcing/

[15] P. La Rocca *et al.*, The Muon Portal Collaboration, "Search for hidden high-Z materials inside containers with the muon portal project," *J. Instrumentation (JINST)*, vol. 9, p. C01056, Jan. 2014.

[16] P. La Rocca *et al.*, "Fabrication, characterization and testing of silicon photomultipliers for the muon portal project," in *Nuclear Instruments & Methods in Physics Research Section A*. : in press, 2015.

[17] D. Lo Presti *et al.*, "OFFSET: Optical fiber folded scintillating extended tracker," *Nuclear Instruments & Methods in Physics Research Section A*, vol. 737, pp. 195–202, Feb. 2014.

[18] S. Riggi *et al.*, The Muon Portal Collaboration, "A large area cosmic ray detector for the inspection of hidden high-Z materials inside containers," in *Proc. the ECRS 2012 Conference*, Moscow, Jul. 2012, vol. 409, pp. 3–7, J. Phys.G (Conf. Series).

[19] S. Riggi *et al.*, The Muon Portal Collaboration, "Muon tomography imaging algorithms for nuclear threat detection inside large volume containers with the muon portal detector," *Nuclear Instruments & Methods in Physics Research Section A*, vol. 728, pp. 59–68, Jul. 2013.